Open Access
Volume 6 Issue 1
Research Article

Journal of Water Engineering and Management
ISSN: 2582-6298

Estimation of Evapotranspiration using Spatial and Ground Based Observations for Irrigated Areas of Allahabad

Avan Kumar[1], D. M. Denis[2], Himanshu Mishra[3]

[1]M.Tech. Student, Department of Irrigation and Drainage Engineering, V.I.A.E.T., S.H.U.A.T.S., Prayagraj, Uttar Pradesh
[2] Professor, Department of Irrigation and Drainage Engineering, V.I.A.E.T., S.H.U.A.T.S., Prayagraj, Uttar Pradesh India
[3]Senior Research Fellow, Department of Irrigation and Drainage Engineering, V.I.A.E.T., S.H.U.A.T.S., Prayagraj, Uttar Pradesh India.,

Article Info

Article History:
Received on: October 29, 2024
Revised on: January 10, 2025
Accepted on: March 5, 2025
Published on: 30 April, 2025
Published by Academic Hope

***Corresponding author** D. M. Denis
Email: derrickmdenis@gmail.com

How to Cite:
Kumar, A., Denis, D. M. and Mishra, H. 2025. Estimation of Evapotranspiration using Spatial and Ground Based Observations for Irrigated Areas of Allahabad, Journal of Water Engineering and Management 6(1): 1-8, DOI: https://doi.org/10.47884/jweam.v6i1pp01-08

Abstract

A comprehensive study to determine the evapotranspiration for irrigated areas of Allahabad, India using Quantum GIS, Grass GIS, Python programming of SEBAL and Cropwat 8 is made for the period of January to May for 4 years (2015-2018). Landsat 8 data, DEM, weather data like rainfall, temperature (min. & max.), relative humidity, solar radiation, wind speed, and observed PET data which are used for the SEBS model. DEM was downloaded from SRTM and Landsat 8 data taken from USGS. The rainfall and temperature data which is collected from department of Forestry and Environment SHUATS Allahabad. The entire study compares ET estimated from SEBS and Penman Monteith single source approach model. SEBS approach for the estimation of ET and the Penman Monteith single source approach method (FAO 56) concludes the average minimum and maximum value of ET is 1.07 to 5.40. and 1.02 to 3.17. The Spatial and ground based observations of the study area during the day concludes the co relation of SEBS ET and Penman Monteith single source approach method (FAO 56) ET have coefficient of determination R^2 = 0.845. Technique were developed for the continuing determination of monthly evapotranspiration from the irrigated areas.

Keywords: SEBAL: DEM; Evapotranspiration: Grass GIS: Penman Monteith.

Introduction

Evapotranspiration (ET) refers to the combined processes of water loss in a given place, comprising both evaporation and plant transpiration. According to Allen et al. (1998), accurately estimating effective management of water resources is significantly dependent on ET. In hydrological research and the design of hydro-technical systems, quantifying water loss due to ET is a fundamental aspect of water balance assessments. However, as noted by Wallace (1995), existing experimental techniques fail to precise assessment of the spatial distribution of ET, even though current measurement tools can provide precise punctual estimates. Understanding and measuring ET is increasingly important in the context of worldwide change research, as it acts as critical role in the Earth's

hydrological and climatic processes.

Prior investigation has concentrated regarding the microclimatic factors influencing evapotranspiration (ET) to establish an analytical framework for comprehending this way. This focus is essential for assessing large areas in worldwide research, necessitating the development of methods that quantitatively address ET measurements at regional, continental, and global scales. Large areas can be evaluated using remotely sensed data, and significant effort has been put into characterizing vegetation using satellite data. There are fundamental connections between spectral reflectance and vegetative traits. Plant biophysical parameters can be defined using spectral transforms thanks to these relationships. Research on grass, soybean, and corn canopies by Ritchie et al. (1971) showed a correlation between the normalized difference vegetation index (NDVI) and several plant canopy metrics, including the percentage of green cover, metabolically active biomass, and the green leaf area index (LAI). In studies by Stern (1965) for safflower and Hinkle et al. (1984) for corn and soybeans, LAI is linked to evapotranspiration. Interestingly, Hinkle et al. (1984) discovered that, up to a LAI of 2.7, ET was proportionate to corn plant density. Until the plants begin to senesce, the crop coefficient stabilizes and remains constant.

An empirical ratio that contrasts observations of crop evapotranspiration with reference crop ET is known as a crop coefficient, allowing for modifications from potential to actual ET depending on environmental factors impacted by solar radiation and climate data (Doorenbos et al., 1977). The seasonal NDVI curve closely matches the coefficient curve for corn's basal crop (Bausch et al., 1987). They concluded that NDVI-derived crop coefficients successfully display crop coefficients in real-time and observed that NDVI reaches its maximum at a LAI of approximately 3.2, which validates findings of Hinkle et al. (1984). Neale et al. (1989) established a link between spectral crop coefficients and corn ET determined by lysimeters to show that reflectance-based coefficients are vulnerable to changes in growth rates caused by various weather conditions. Leprieur (1989) investigated the relationship between LAI and NDVI further and discovered that, in investigations involving mixed vegetation areas using data from an airborne visible/infrared imaging spectrometer, NDVI saturation happened at a LAI of 3. Up to a LAI of 3, there is a generally linear link between LAI and ET, NDVI, and crop coefficients; beyond that, increases in LAI result in declining returns in these three interconnected parameters. This pattern implies that an appropriately calibrated NDVI can offer direct ET-related information.

Almhab et al. (2007) obtained the NDVI from TM data and evapotranspiration (ET) observations across a large area and utilized multiple meteorological stations in arid regions. Their findings indicated that areas exhibiting low NDVI values were associated with lower ET rates. The current focus in this field is primarily on enhancing the reliability of radiant flux measurements. Although surface albedo can be reliably determined using standard sensors, which facilitates the computation of shortwave net radiation, more specialized sensors are required to accurately assess the longwave component of the radiation balance. Furthermore, estimates of upwelling radiation components can be derived from surface albedo and temperature, while downwelling components rely on meteorological data inputs. In order to calculate soil heat flux, Bastiaanssen (1995) suggested utilizing spectral indices or semi-empirical equations that integrate Rn, surface albedo, surface temperature, NDVI, and area-averaged surface albedo. This is done by dividing ground heat flux (G) by net radiation (Rn).

The study focuses on the parameterization of turbulent fluxes, emphasizing two key parameters: Aerodynamic resistance (rah), which is important for momentum and heat transport, and the LAI, which is derived from NDVI. While related techniques utilize image context for deriving equations from range data, these methods are limited by area and specific image conditions, hindering process automation. The aim is to showcase the application of NDVI for estimating evapotranspiration (ET), leveraging data and methods from the NWRA utilized in the relevant study areas. In practice, most evapotranspiration estimation techniques begin with identifying the major controlling components such as net radiation, aerodynamic factors, and soil-plant interactions, followed by assessing or measuring these components individually. The derived values are then combined and expressed through a surface energy-balance relationship to obtain the final evapotranspiration estimate.

Materials and Methods

Study Area

The study was conducted at Sam Higginbottom University of Agriculture, Technology & Sciences in Allahabad, which has geographic coordinates of 24°47'N and 81°09'E. The study area covers 5246 km² and lies at an elevation exceeding 90 m above sea level. The region obtains an average annual rainfall of approximately 934

mm with 85% occurring between May and September. This rainfall level is insufficient to support the growth of most agricultural crops, necessitating irrigation. Surrounding the irrigated fields are dry areas, indicative of the semi-arid ecology of the region. The strong network of canal as well as ground water is source of irrigation which irrigates 125568 ha area under cultivation. There are 1006 number of government tube wells by which 19438 ha area is irrigated in the study area. The Allahabad city is situated in the southern part of Uttar Pradesh and this borders Pratapgarh to the north, Bhadohi to the east, Rewa to the south, and Kaushambi to the west (Fig. 1). The city covers an area of 63.07 km² and includes several suburbs. Multiple municipalities govern the city and its surrounding areas, while the Allahabad City Council administers a major portion of the Allahabad District. Notably, in 2011, Allahabad was recognized as the world's 130th fastest growing city.

Fig. 1. Study map area

Study Period

It is desirable to conduct the research on estimation of evapotranspiration in the part of year basis, i.e. for the period of five months of every year from 2015 to 2018 which consists maximum solar radiation period and minimum solar radiation period (Sunshine hours) because generally, the periods for study in such situations will be from the time of maximum evapotranspiration to the time of minimum evapotranspiration as the maximum solar radiation period and from the time of minimum solar radiation. The research periods were taken as January, February, March, April and May.

Surface Energy Balance Equation

Theoretical basis of SEBAL

The SEBAL model estimates evapotranspiration (ET) using meteorological data and satellite imagery. Specifically, the model uses surface energy balance principles and calculates an instantaneous ET flux based on the precise time the satellite takes the image. It uses the surface energy budget equation, which is given as follows, to calculate this ET flux for every pixel in the image:

$$\lambda ET = R_n - G - H \quad \text{…….. (1)}$$

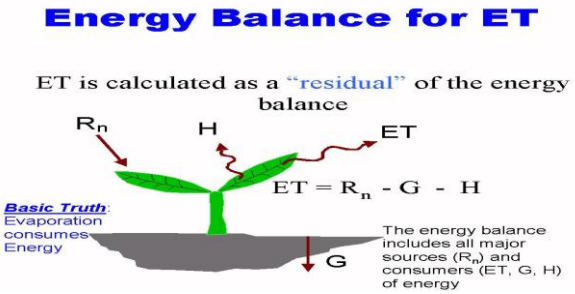

Fig. 2 Surface energy balance

The amount of radiant energy available at the surface level is known as the net radiation flux at the surface (Rn). It is determined by deducting all incoming radiant fluxes from all outgoing radiant fluxes, as per the surface radiation balance equation:

$$R_n = R_{S\downarrow} - \alpha R_{S\downarrow} + R_{L\downarrow} - R_{L\uparrow} - (1-\varepsilon_o) R_{L\downarrow} \quad \text{…….. (2)}$$

Net surface radiation = gains – losses

$$R_n = (1 - \alpha) R_{S\downarrow} + R_{L\downarrow} - R_{L\uparrow} - (1-\varepsilon_o) R_{L\downarrow}$$

Equation (2) illustrates the relationship between surface albedo (α), the ratio of incident to reflected radiant flux across the solar spectrum, and the shortwave radiation at the surface ($R_{S\downarrow}$). Surface albedo is calculated using satellite imagery that offers information on spectral radiance in various satellite bands. The relative Earth-Sun distance, atmospheric transmissivity, solar constant, and solar incidence angle are all taken into account when calculating incoming shortwave radiation ($R_{S\downarrow}$). Moreover, a modified Stefan–Boltzmann equation that takes into account atmospheric transmissivity and a chosen reference surface temperature is used to calculate incoming longwave radiation ($R_{L\downarrow}$). Outgoing longwave radiation ($R_{L\uparrow}$) is computed using the Stefan-Boltzmann equation with a calculated surface emissivity and surface temperature. Surface temperatures are computed from satellite image information on thermal radiance. The ratio of a surface's actual radiation emission to that of a black body at the same temperature is known as surface emissivity. SEBAL calculates emissivity as a vegetation

index function. The amount of incoming longwave radiation reflected by the surface is represented by the last term in Equation (2), $(1 - \varepsilon_0) R_{L\downarrow}$.

The residual energy for evapotranspiration (λET) in the SEBAL model is computed by deducting the net radiation flux (Rn) from the sensible heat flux (H) and the soil heat flux (G). While the sensible heat flux is calculated using information from temperature variations, wind speed, and surface roughness, the soil heat flux is calculated using vegetation indices, surface temperature, and albedo. To account for atmospheric instability brought on by surface heating, the model uses an iterative approach. To calculate the instantaneous evapotranspiration (ET) rates in mm/hr, divide all pixel's latent heat flux (λET) by its latent heat of vaporization (λ). Based on local weather data, these ET measurements are then converted to daily or seasonal values in relation to reference crop ET (ETr), which is the evapotranspiration from fully covered alfalfa or clipped grass surfaces. By incorporating elements like elevation, slope, and aspect, SEBAL's use is further extended to mountainous regions, where it offers extremely accurate ET estimates, particularly in flat agricultural areas.

SEBAL is a powerful, physics-based analytical method that focuses on assessing surface energy balance components. Actual evapotranspiration (ETa), a residual value obtained from the energy balance, can be calculated using this method. The methodology contributes to a thorough understanding of energy interactions within terrestrial ecosystems by following the law of conservation of energy, which describes the dynamics of energy input, release, and storage across the Earth's surface.

$$R_n = G + H + \lambda ET \ (W/m^2) \quad \text{..... (3)}$$

By supplying the energy required for a number of fluxes, including soil heat flux (G), sensible heat flux (H) exchanged with the atmosphere, and latent heat flux (λET), which is connected to moisture transfer, net radiation flux (Rn) plays a critical role in the Earth's surface energy balance. There are various ways to quantify these individual energy components in order to estimate net radiation. In general, net radiation is determined by the interaction of incoming and outgoing shortwave and longwave radiation at the surface of the Earth.

$$R_n = R_{S\downarrow}(1-\alpha) + R_{L\downarrow} - R_{L\uparrow} - R_{L\downarrow}(1-\varepsilon_0) \ (W/m) \quad \text{.....(4)}$$

$R_{S\downarrow}$(W/m²) indicates the amount of solar radiation, both direct and diffuse, that reaches the Earth's surface. The parameter α denotes surface albedo, which measures the fraction of incoming shortwave radiation that is reflected back by the surface. Outgoing longwave radiation from the Earth's surface to the atmosphere is represented by $R_{L\downarrow}$, while $R_{L\downarrow}$ also denotes incoming longwave thermal radiation from the atmosphere. Additionally, ε_0 represents surface emissivity, defined as a dimensionless ratio that compares the radiant emittance of a grey body to that of an ideal black body. Surface albedo is computed by converting satellite-observed spectral reflectance values into broadband reflectance and then combining these reflectances across relevant satellite bands using sensor-specific weighting coefficients.

$$\alpha = \frac{\alpha_{toa} - \alpha_{path\_radiance}}{{\tau_{sw}}^2} \quad \text{..... (5)}$$

The average percentage of solar radiation that returns to the satellite sensor before it reaches the Earth's surface is called αpath. Typical values range from 0.025 to 0.04, with SEBAL typically using a default value of 0.03. After the effects of absorption and reflection are eliminated, atmospheric transmissivity (τ_{sw}) is the percentage of incoming solar radiation that successfully travels through the atmosphere. The estimation of τ_{sw}, which takes into account both diffuse and direct solar radiation that reaches the ground, is covered in the text. This estimate is based on an empirical relationship that depends on elevation, especially in situations with dry air and clear skies.

$$\tau_{sw} = 0.75 + 2.\ 10^{-5} \quad \text{.....(6)}$$

the albedo (α_{toa}) at the top of the atmosphere is determined using

$$\alpha_{toa} = \Sigma\ (\omega_\lambda \times \varrho_\lambda) \quad \text{..... (7)}$$

In this formulation, $\varrho\lambda$ indicates the reflectivity for each spectral band, while $\omega\lambda$ represents the associated weighting coefficient, which is derived using Equ. (8) to evaluate the contribution of each band to the broadband surface albedo.

$$w_\lambda = \frac{ESUN\lambda}{\Sigma ESUN\lambda} \quad \text{.....(8)}$$

Each spectral band's weighting coefficient is denoted by

ωλ, and its mean solar exo-atmospheric irradiance, expressed in W/m²/µm, is denoted by ESUNλ We compute the reflectivity for each band (ϱλ) using Equ. (9) for Landsat images:

$$\varrho\lambda = \frac{\pi.L\lambda}{ESUN} \quad \ldots\ldots(9)$$

The inverse squared relative Earth-Sun distance (dr) is calculated using the sequential day of the year (DOY) and converted to radians using the formula (DOY × 2π / 365). Lλ stands for each band's spectral radiance. The cosine of the angle of solar incidence from the vertical (nadir) is called cos θ. For both Landsat 5 and Landsat 7, we use Equ. (10) to calculate each band's spectral radiance (Lλ), which is the outgoing radiant energy that the satellite at the top of the atmosphere measured.

$$L_\lambda = \left(\frac{L_{MAX}-L_{MIN}}{QCAL_{MAX}-QCAL_{MIN}}\right) \times (DN - QCAL_{MIN}) + L_{MIN} \ldots (10)$$

LMIN and LMAX are the calibration constants that correspond to the lowest and maximum spectral radiance values for the corresponding band, DN is the digital number recorded for each pixel, and Lλ is expressed in W/m²·sr·µm. QCALMIN and QCALMAX represent the minimum and maximum rescaled radiance values in digital numbers. For Landsat 8, the digital number range is standardized with QCALMAX = 255 and QCALMIN = 0; therefore, Equ. (10) is modified accordingly to accommodate this calibration range.

$$L_\lambda = \left(\frac{L_{MAX}-L_{MIN}}{255}\right) \times DN + L_{MIN} \quad \ldots. (11)$$

Landsat 8 ETM+ images provide the calibration constants required for radiometric processing within the header files associated with each scene. Using these calibration parameters, we calculate the spectral radiance (Lλ) for each band using Equ. (12), which converts the digital number values of each pixel into physically meaningful radiance units.

$$L_\lambda = gain \times DN + offset \quad \ldots\ldots. (12)$$

The NDVI is then calculated as the ratio of the red band's (ϱ3) and near-infrared band's (ϱ4) reflectivity differences to their sum, as shown in Equ. 13.

$$NDVI=(\varrho_4-\varrho_3)/(\varrho_4+\varrho_3) \quad \ldots\ldots. (13)$$

The modified Plank equation, Equ. (14), is used to determine the surface temperature (Ts).

$$T_S = \frac{K_2}{\ln\left(\frac{\varepsilon_{NNB}K_1}{R_C}+1\right)} \quad \ldots\ldots\ldots (14)$$

We compute the effective at-satellite temperature (Ts) in Kelvin using the calibration constants K_1 and K_2 provided for Landsat imagery. To obtain Ts, we first calculate the corrected thermal radiance from the surface (Rc), and then incorporate the narrow-band emissivity ($\varepsilon_{nn\beta}$), which takes a value of 0.98 for NDVI > 0 and 0.99 for NDVI < 0. The units of Rc remain consistent with those of K_1, as required for the temperature conversion. Equ. (15) is used to compute the modified thermal radiance to the surface (Rc).

$$R_c = \frac{L_{t,b}-R_p}{\tau_{NB}} - (1-\varepsilon_{NB})R_{sky} \quad \ldots\ldots\ldots.(15)$$

In this equation, **Rc** represents the surface-corrected thermal radiance (W/m²·sr·µm), while **εNB** denotes the narrow-band emissivity. The term **Lt,b** corresponds to the measured spectral radiance (W/m²·sr·µm), **Rp** denotes the path radiance within the 10.4–12.5 µm range, and **Rsky** refers to the downward narrow-band thermal radiation under clear-sky conditions (W/m²·sr·µm). The parameter **τNB** represents the narrow-band atmospheric transmissivity for the 10.4–12.5 µm wavelength region. The soil heat flux (G) is a representation of the rate of heat conductivity and storage in the ground. The researchers came up with the following empirical relationship for G during their study of Turkey's irrigated agricultural areas:

$$G = R_n T_s/\alpha(.0038\alpha + .0074\alpha^2)(1 - .98NVDI^4)(W/m^2) \quad \ldots\ldots..(16)$$

Here, **α** represents the surface albedo (dimensionless), T denotes the surface temperature (°C), and NDVI refers to the normalized difference vegetation index. Brutsaert et al. highlight that estimating the sensible heat flux (H) is the most difficult component of physically based remote-sensing models. In SEBAL, this challenge is more pronounced because several parameters required for computing H are difficult to derive accurately. The model estimates sensible heat flux using the heat-transport equation shown in Eq. (17), which is formulated from Monin-Obukhov similarity theory and accounts for atmospheric stability conditions as well as the aerodynamic resistance to heat transfer (rah).

$$H = (\varrho cpdT)/rah \quad \ldots (17)$$

This section outlines the variables affecting the estimation of sensible heat flux (H), such as air density (ϱ), specific heat capacity of air (cp), the temperature gradient (dT) between the land surface and air, and aerodynamic resistance to heat transfer (rah). The latter is influenced by wind speed, atmospheric stability, and surface roughness characteristics. In SEBAL, rah is determined via an iterative method. After determining Rn, G, and H, SEBAL computes the latent heat flux as the last component of the surface energy balance. Next, the latent heat flux is expressed as follows by rearranging Equ. (18):

$$\lambda ET = Rn - G - H(W/m2) \quad \ldots (18)$$

The latent heat of vaporization (λ) is divided by a particular expression to find the instantaneous evapotranspiration (ET). The instantaneous latent heat flux, which is the residual component of the surface energy budget, is then used to calculate the instantaneous evaporative fraction (EF). Using Equ. (19), the evaporative fraction is calculated.

$$EF = \frac{\lambda E}{\lambda E + H} = \frac{\lambda E}{R_n - G_o} \quad \ldots\ldots (19)$$

EF is the ratio of real to crop evaporative demand when atmospheric moisture and soil moisture availability are equal. Even while H and E fluxes may fluctuate during the day, the instantaneous EF is comparatively constant, thus we utilize it to calculate the daily EF. The slight discrepancy between the 24-hour integrated energy-balance EF and the instantaneous EF at the time of satellite overhead can be disregarded, as mentioned by Farah et al. We simplify the net accessible energy ($R_n - G_0$) to net radiation (Rn) for durations of one day or more by ignoring G_0.

Hydrological applications need daily LE or daily ET, whereas the SEBAL model estimates latent energy (LE) in W m^{-2} at the time of satellite overhead. This is achieved by using the evaporative fraction (EF) to extrapolate the immediate LE to a full-day value. As stated in Eq. (20), we can utilize EF to scale the instantaneous LE to daily ET since it is almost constant during the day.

$$EF_{inst} = \frac{R_n - G - H}{R_n - G} = \frac{LE_{inst}}{LE_{inst} + H_{inst}} \approx EF_{24} \quad \ldots. (20)$$

Therefore, the daily evapotranspiration rate (mm/day) is obtained by multiplying the instantaneous evaporative fraction (EFinst) derived from SEBAL by the total daily available energy. This procedure is expressed in **Equations (21) and (22)**.

$$LE_{24} = EF_{inst} \times (R_{n24} - G_{24}) \quad \ldots\ldots. (21)$$

$$ET_{24} = \frac{EF_{inst} \times (R_{n24} - G_{24})}{\lambda} \quad \ldots\ldots. (22)$$

CROPWAT 8.0 Model

The FAO's Land and Water Development Division developed the CROPWAT decision support system to enhance irrigation planning and management. Because it offers a helpful platform for computing reference evapotranspiration, crop water requirements, and irrigation demand, it is particularly helpful for creating and managing irrigation plans. The software enables users to develop recommendations for optimizing irrigation practices, create irrigation schedules under varying water-supply conditions, and assess crop performance in both rainfed and deficit-irrigated environments. Its computational procedures are based on FAO Irrigation and Drainage Papers No. 24 and No. 33, which outline crop water-requirement methodologies and the relationship between crop yield and water availability. Furthermore, CROPWAT generates irrigation schedules and evaluates rainfed versus irrigated conditions using a daily soil-water balance that accommodates diverse management practices and water-supply scenarios Minimum and maximum temperatures are measured in degrees Celsius (°C), while sunshine hours are recorded in hours (hrs). Wind speed is expressed in km/day, and relative humidity is given as a percentage (%). Geographic coordinates include latitude and longitude in degrees, minutes, and seconds (DMS). Altitude is measured in meters (metre). The Cropwat model outputs include solar radiation in MJ/m^2/day and reference evapotranspiration (ET0) measured in mm/day.

$$ET_o = \frac{0.408\,\Delta\,(R_n - G) + Y\frac{900}{T+273}(e_s - e_a)}{\Delta + Y\,(1 + 0.34\,u_2)} \quad \ldots\ldots (23)$$

Results and Discussion

This research successfully demonstrated a method for integrating remotely sensed data and a crop ET simulation for monitoring crop growth and predicting water management. In this phase of the research LANDSAT 8 (OLI) data were used to assess wheat yield

in irrigated area of Allahabad and the model simulation were adjusted to produce the accuracy that matched with estimated Cropwat ET in irrigated area of Allahabad. LANDSAT 8 data at every 16 days' interval has been taken-(Dated 06/01/2015, 23/02/2016, 11/03/2015, 28/04/2015, 23/05/2015; 11/01/2017, 28/02/2017, 16/03/2017, 01/04/2017, 19/05/2017 and 30/01/2018, 15/02/2018, 19/03/2018, 04/04/2018, 06/05/2018) and the vegetation indices were created (NDVI, SAVI, EVI) for every day of pass. SEBS_ET shows a strong positive linear relationship with Cropwat_ET ($R^2 \approx 0.85$), indicating good agreement between satellite-based energy-balance and FAO-56 model-based ET estimates. SEBS slightly overestimates ET at low values but aligns closely with Cropwat at higher ET, demonstrating overall consistency and reliability of SEBS for operational ET assessment (Fig.2). The ET distribution in May 2018 indicates high evapotranspiration along river corridors and moist agricultural fields, reflecting high water availability. In contrast, the upland and dry plateau regions show very low ET due to moisture scarcity and stressed vegetation. The pattern clearly represents the typical pre-monsoon condition of the region with strong spatial variability controlled by hydrometeorology and land cover (Fig. 3). The January 2018 ET map shows a predominantly low evapotranspiration regime (<1 mm/day) over most of the landscape, driven by cool temperatures and reduced net radiation. Moderate ET is restricted to moist cropland and mixed vegetation patches, while the highest ET values around rivers and waterlogged areas reflect evaporation from open water even during winter (Fig. 4). Overall, the spatial pattern confirms strong energy limitation of ET during the winter season.

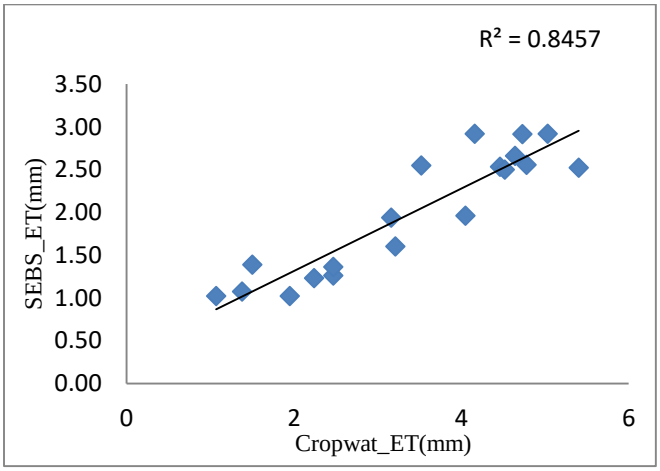

Fig. 2 Simulation results of SEBS_ET and CROPWAT evapotranspiration

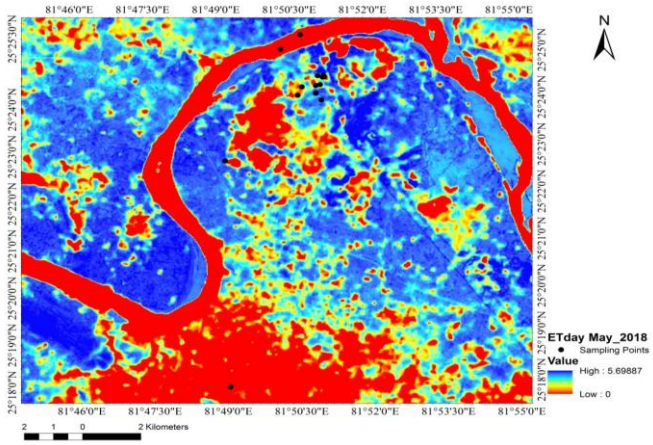

Fig. 3 ET values obtained for the study area in May 2018

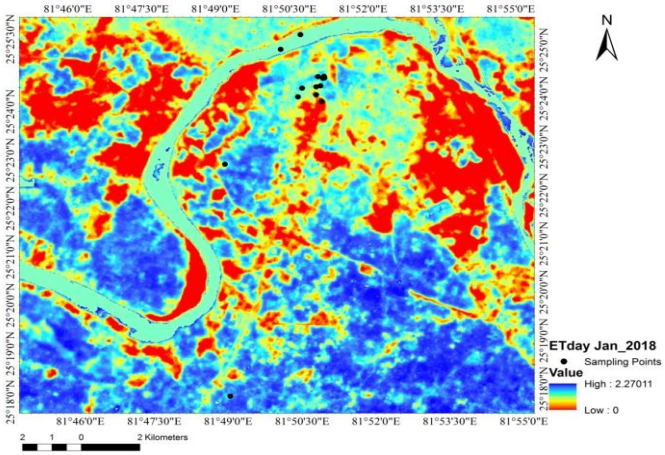

Fig. 4 ET values obtained for the study area in January 2018

Conclusions

This study's primary goal was to simulate the Cropwat_ET using spatially distributed evapotranspiration as its input, estimated from satellite remote sensing, and to track how the simulation results changed when satellite-based SEBS_ET and Cropwat_ET estimated from 15 sampling points were applied. The (SEBS) algorithm were used to estimate daily evapotranspiration (ET) in the study area for both dry and wet seasons. This estimation was derived from satellite data provided by Landsat 8 and supplemented by meteorological station data, although some Landsat 8 products were compromised due to cloud cover. The ET calculations were performed for each land cover class, enabling an assessment of the seasonal variation in ET

specific to these classes. The results indicated that the ET calculated from the SEBS algorithm were realistic and aligned well with the expected seasonal variability in the region. Notably, the highest daily ET was recorded in May, reaching 5.17 mm/day during the wet season, while the lowest ET occurred in January, at 1.02 mm/day, representative of the dry season.

Additionally, the study area's evapotranspiration was computed using Cropwat 8. ETo was estimated from the meteorological station data. Average ETo from these stations had taken for the sensitivity analysis, calibration and validation of the SEBS_ET to the Cropwat_ET simulation for the years 2015 to 2018. This research successfully demonstrated a method for integrating remotely sensed data and a crop ET simulation for monitoring crop growth and predicting water management. In this phase of the research LANDSAT 8 (OLI) data were used to assess wheat yield in irrigated area of Allahabad and the model simulation were adjusted to produce the accuracy that matched with estimated Cropwat ET in irrigated area of Allahabad. LANDSAT 8 data at every 16 days' interval has been taken (Dated 06/01/2015, 23/02/2016, 11/03/2015, 28/04/2015, 23/05/2015;11/01/2017, 28/02/2017, 16/03/2017, 01/04/2017, 19/05/2017 and 30/01/2018, 15/02/2018, 19/03/2018, 04/04/2018, 06/05/2018) and the vegetation indices were created (NDVI, SAVI, EVI) for every day of pass.

Data Availability Statement

The datasets generated during the current study are available from the corresponding author on reasonable request.

Conflict of Interest

The authors declare that they have no known competing financial interests or personal relationships that could have appeared to influence the work reported in this paper.

Funding

This research received no external funding.

References

Allen, G. R., Pereira, L. S., Raes, D. and Smith, M. 1998. Crop evapotranspiration—Guidelines for computing crop water requirements. FAO Irrigation and Drainage Paper 56, FAO, Rome.

Allen, R. G. 2000. REF-ET: Reference evapotranspiration calculation software for FAO and ASCE standardized equations. University of Idaho.

Bastiaanssen, W. G. M. 1995. Regionalization of surface flux densities and moisture indicators in composite terrain: A remote sensing approach under clear skies in Mediterranean climates. Wageningen Agricultural Research Department.

Bastiaanssen, W. G. M., Menenti, M., Feddes, R. A. and Holtslag, A. A. M. 1998. A remote sensing surface energy balance algorithm for land SEBAL. 1. Formulation. Journal of Hydrology, 212–213: 198–212.

Cristina Serban Gherghina, Maftei, C. and Barbulescu, A. 2007. Estimation of evapotranspiration using remote sensing data and grid computing: A case study in Dobrogea, Romania. Latest Trends on Computers II, 596–601.

Denis, D. M. 2013. Irrigation performance assessment using SEBS and SCOPE: A case study of Tons pump canal command in India. MSc Thesis, University of Twente, Faculty of Geo-Information and Earth Observation ITC.

Doorenbos, J. and Pruitt, W. O. 1977. Crop water requirements. FAO Irrigation & Drainage Paper 24 Revised, FAO, Rome.

IEEE. 1990. Using spatial context in satellite data to infer regional scale evapotranspiration. IEEE Geoscience and Remote Sensing Society.

Marica, A. 2005. *CROPWAT Software*. FAO. http://www.fao.org/waicent/faoinfo/agricult/agl/aglw/cropwat.htm

Ritchie, J. T. and Burnett, E. 1971. Dryland evaporative flux in a subhumid climate: II. Plant influences. Agronomy Journal 63: 56–62.

Trenberth, K. E. and Asrar, G. R. 2014. Challenges and opportunities in water cycle research: WCRP contributions. In The Earth's Hydrological Cycle, 515–532.

Xin, S. 2007. Regional evaporation over the arid inland Heihe River Basin in Northwest China. MSc thesis, International Institute for Geo-Information Science and Earth Observation.

Yang, D., Chen, H. and Lei, H. 2010. Estimation of evapotranspiration using a remote sensing model over agricultural land in the North China Plain. International Journal of Remote Sensing 31(14): 3783–3798.

Zhao-Liang, L., Tang, R., Wan, Z., Bi, Y., Zhou, C., Tang, B., Yan, G. and Zhang, X. 2009. A review of current methodologies for regional evapotranspiration estimation from remotely sensed data. Sensors 9 5, 3801–3853. doi:10.3390/s90503801